Effect of pressure on crystal-field transitions of Nd-doped $YLiF_4$

F. J. Manjón,[1,*] S. Jandl,[2] K. Syassen,[1,†] and J. Y. Gesland[3]
[1]*Max-Planck-Institut für Festkörperforschung, Heisenbergstrasse 1, D-70569 Stuttgart, Germany*
[2]*Centre de recherche sur les propriétés électroniques des matériaux avancés Université de Sherbrooke, Sherbrooke, Québec, Canada J1K2R1*
[3]*Université du Maine Cristallogenese, 72085 Le Mans, CEDEX 9, France*
(Received 12 April 2001; revised manuscript received 25 June 2001; published 20 November 2001)

Luminescence spectra of Nd^{3+}-related crystal field transitions of $YLiF_4$ with 2% Nd doping were measured as a function of hydrostatic pressure at $T=5$ K. Specifically, transitions from the $^4F_{3/2}(1)$ excited level to the $^4I_{9/2}$ and $^4I_{11/2}$ states have been studied. Most of the isolated-ion transitions show a redshift with increasing pressure up to 10 GPa, resulting from a decrease of the Slater free-ion and spin-orbit parameters and an increase of the crystal field interactions as pressure increases. Spectra near the $^4F_{3/2}(1)$ to $^4I_{9/2}(1)$ ground state emission evidence the presence of satellite lines assigned to Nd^{3+}-Nd^{3+} ion pairs coupled by magnetic dipolar interaction. The splitting between the $^4F_{3/2}(1)\rightarrow{}^4I_{9/2}(1)$ isolated-ion emission and its satellites is found to increase with pressure. This effect is attributed to stronger magnetic coupling as the Nd^{3+} pair distances decrease. The pressure dependence of the $^4F_{3/2}(1)$ to $^4I_{9/2}(1)$ luminescence energy indicates subtle structural changes of the scheelite phase at around 5.5(5) GPa. Major spectral changes observed near 10 GPa indicate a first-order structural phase transition.

DOI: 10.1103/PhysRevB.64.235108 PACS number(s): 71.70.Ch, 62.50.+p, 42.55.Rz, 71.70.Gm

I. INTRODUCTION

Yttrium lithium fluoride is a common host material for rare-earth ion lasers. The near-infrared emissions of Nd-doped $YLiF_4$ at 1047 and 1053 nm are widely used as laser lines.[1–5] Diode pumping of doped $YLiF_4$ and isostructural $GdLiF_4$ has opened the possibility for developing powerful solid state lasers with emission in the visible after frequency conversion. The effect of doping with Nd^{3+} ions and the related laser action and up-conversion properties have been studied in detail.[6–11]

At ambient conditions, $YLiF_4$ crystallizes in the tetragonal scheelite-type structure with space group $I4_1/a$ (C_{4h}^6) and four molecules per unit cell.[12] The structure [see Fig. 1(a)] may be considered as a tetragonally distorted superstructure of cubic CaF_2. An ordered occupation of cation positions by Y^{3+} and Li^+ ions and a displacement of anions leads to a doubling of the cubic unit cell (with tetragonal $c/a>2$) along one of the cubic axes. Y^{3+} ions are coordinated by eight F^- ions (four at 2.248 Å, four at 2.30 Å) forming YF_8 polyhedra with S_4 site symmetry for Y. Li^+ ions are surrounded by four equally spaced F^- ions at 1.74 Å distance forming distorted LiF_4 tetrahedra. Each Y^{3+} (Li^+) ion has four Y^{3+} (Li^+) second nearest neighbors at the same distance, i.e., the Y and Li sublattices represent two interpenetrating diamondlike nets. On doping, Nd^{3+} ions substitute for Y^{3+}. Studies of Nd^{3+} crystal field (CF) excitations in $YLiF_4$ have resulted in the determination of several sets of parameters for a CF Hamiltonian of D_{2d} symmetry as an approximation to the actual S_4 symmetry.[13,14] Satellites of the CF excitations have been observed and attributed to Nd-F-Nd superexchange interaction[15] and more recently to ferromagnetically coupled Nd^{3+} pairs in which the Nd^{3+}-Nd^{3+} ferromagnetic interaction does not affect substantially the crystal field at each ion.[16–18] Coupled-pair luminescence may give rise to intrinsic bistability and hysteresis resulting from a cooperative effect due to ion-ion coupling within the dimer as predicted by Bowden and Sung[19] and reported by Hehlen *et al.* in different systems.[20] In order to better understand the ion-ion coupling mechanisms, a variation of interatomic distances by pressure-tuning is of considerable interest.

Two optical high-pressure studies of $YLiF_4$ have been reported recently. Luminescence measurements of $YLiF_4$:Eu up to 15 GPa ($T=300$ K) indicate a pressure-induced phase transition to a low-symmetry crystal structure at around 10 GPa.[21] A Raman study of $YLiF_4$ as a function of temperature and pressure (0–20 GPa) showed clear changes in the frequency-versus-pressure slopes of some modes at around 7 GPa.[22] This behavior was attributed to a stiffening of the tetrahedral LiF_4 group rather than to a structural phase transition.

In this paper we report the pressure dependence of the $^4F_{3/2}(1)\rightarrow{}^4I_{9/2}$ and $^4F_{3/2}(1)\rightarrow{}^4I_{11/2}$ CF emission energies of Nd^{3+} in $YLiF_4$ measured at low temperatures. A simplified energy level scheme of Nd^{3+} in $YLiF_4$ is shown in Fig. 1(b). The CF Hamiltonian lifts the $2J+1$ degeneracy of the $^{2S+1}L_J$ states. For the $^4I_{9/2}$ ground state the crystal-field interaction gives rise to five Stark levels (Kramers doublets), labeled as 1,2, . . . , and the excited $^4I_{11/2}$ and $^4F_{3/2}$ states split into six and two doublets, respectively. The pressure dependence of Nd^{3+} CF transitions can be used to improve parametrized CF Hamiltonians. In addition to the isolated-ion emissions, we have observed satellites attributed to Nd^{3+} pair interactions. The Nd^{3+} pair luminescence under pressure is of interest because it may lead to a better description of the dominant pair interaction. Finally, the study of the

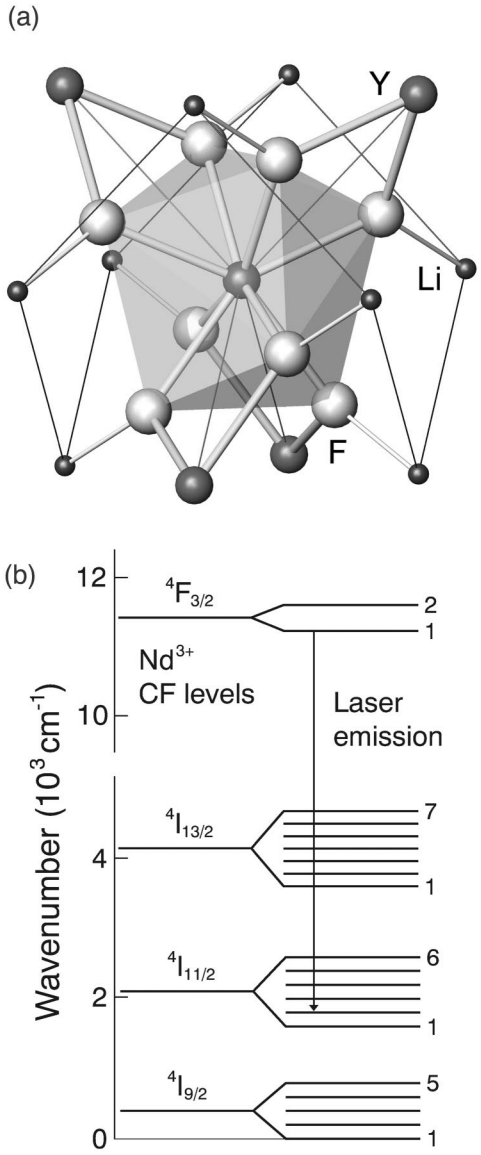

FIG. 1. (a) Atomic arrangement in the scheelite-type structure of $YLiF_4$. Only one half of the tetragonal unit cell is shown. (b) Energy level diagram (schematic) of Nd^{3+} in $YLiF_4$. Stark levels are numbered in order of increasing energy.

pressure dependence of CF luminescence can provide indications for structural changes in $YLiF_4$ under pressure.

II. EXPERIMENTAL DETAILS

The $YLiF_4$ crystals used in this study were doped with 2% of Nd atoms. A single crystal sample ($100\times100\times30$ μm^3) was inserted in a diamond anvil cell (DAC). Helium was used as pressure transmitting medium to ensure hydrostatic pressure conditions. Low-temperature measurements ($T=5$ K) were performed in a continuous-flow helium cryostat in which the DAC was inserted. The 0–12 GPa pressure-range was studied. Change of pressure was always performed above the helium melting temperature in order to avoid nonhydrostatic conditions. The pressure was measured by the ruby luminescence method[23,24] using a temperature correction according to Ref. 25. The lines at 5145 and 4965 Å of an Ar^+-ion laser were used for excitation of the Nd^{3+} ions luminescence. Sample was oriented along the *c* axis and excitation was performed in the $\mathbf{E}\perp\mathbf{c}$ configuration. Scattered light was analyzed by a single-grating spectrometer (0.64 m focal length) equipped with a nitrogen-cooled germanium detector and a GaAs photomultiplier. Spectral resolutions were 1.1 cm^{-1} (100 μm slit width) in the 9500 cm^{-1} range and 0.16 cm^{-1} (10 μm slit width) in the 11 500 cm^{-1} range. Argon and neon plasma lines were used to calibrate the spectra.

III. RESULTS AND DISCUSSION

A. $^4F_{3/2}(1)\rightarrow{}^4I_{9/2}(1)$ emission

We first consider the $^4F_{3/2}(1)\rightarrow{}^4I_{9/2}(1)$ (ground state) emission. Figure 2(a) shows selected luminescence spectra corresponding to this emission at different pressures. An Ar^+-ion laser plasma line present in all high-pressure spectra has been used for spectral calibration. With increasing pressure, the luminescence intensity from the sample showed a continuous decrease. Above 7.5 GPa spectra were excited with the 4965 Å laser line instead of the 5145 Å line, which gave higher intensity. At ambient pressure the luminescence spectrum consists of a central band at 11 538.76 cm^{-1} (the isolated-ion emission) and satellites attributed to several types of ferromagnetically coupled Nd^{3+}-Nd^{3+} pairs with exchange coupling values $J_1=0.8$, $J_2=1.6$, and $J_3=3.1$ cm^{-1}.[17] In this model, for each ground-state exchange-coupled pair, a doublet of lines is expected at energies $E^i+J/2$ and E^i-$3J/2$, where E^i refers to the isolated-ion transition and $J>0$ represents a ferromagnetic Nd^{3+}-Nd^{3+} pair exchange energy. As pressure increases the maximum of the central band first shifts to lower energies and then, above 5.5(5) GPa, exhibits a blueshift. New peaks appear in spectra taken above 10.3 GPa. At 11.2 GPa none of the original peaks remains. Instead, a rather broad luminescence band appears.

We have fitted the spectra around the $^4F_{3/2}(1)\rightarrow{}^4I_{9/2}(1)$ transition by a superposition of Voigt profiles. These are Lorentzians convoluted by a Gaussian with a FWHM corresponding to the spectrometer resolution as determined from the widths of argon and neon calibration lines. In Fig. 2(b) we present the corresponding energies of the isolated-ion emission and its satellites as a function of pressure. The numerical values of energy pressure coefficients for the range up to 5 GPa are listed in Table I. The solid symbols in Fig. 2(b) represent energies of well-resolved peaks. The open symbols indicate energies of three additional Voigt lines used to fit the high-energy tail of the isolated ion band. In the spectra taken at low pressures ($P<3$ GPa) two of the high-energy satellites (assigned as 1/2 J_2 and 1/2 J_3) are clearly resolved and an additional component (1/2 J_1) is needed to account for the spectral profile. The satellites broaden somewhat at higher pressures. Thus, the analysis of spectra at higher pressures is based on the reasonable assumption that the high-energy tail of the

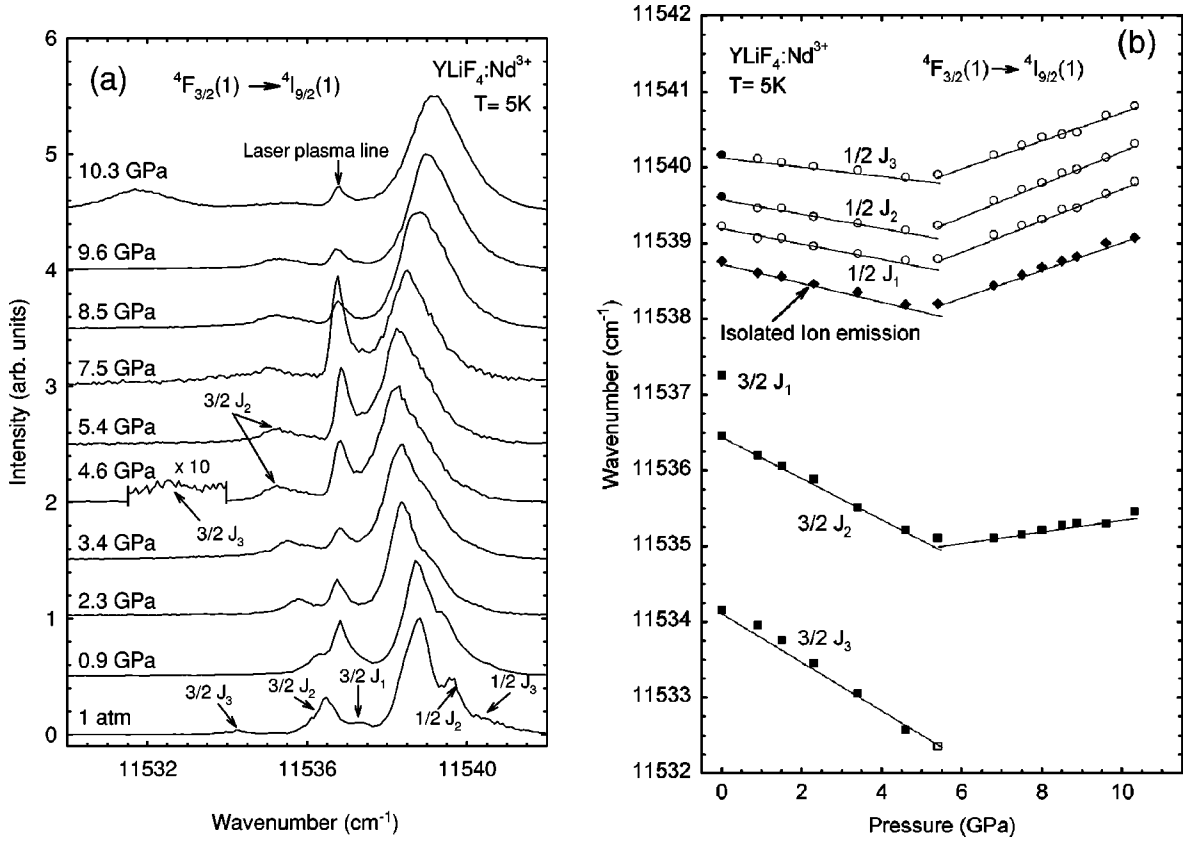

FIG. 2. (a) Luminescence spectra at energies near the $^4F_{3/2}(1) \rightarrow {}^4I_{9/2}(1)$ crystal-field transition of Nd^{3+} in $YLiF_4$ at different pressures. The observed satellite peaks are assigned according to theoretical calculations of exchange interactions (see text). (b) Energies of the isolated-ion $^4F_{3/2}(1) \rightarrow {}^4I_{9/2}(1)$ transition and its satellites as a function of pressure. Solid symbols refer to peaks which are well resolved in the spectra. Open symbols indicate energies of additional Voigt lines used in fitting the spectra.

TABLE I. Ambient-pressure energies E_0^i and frequency pressure coefficients $dE^i/d\mathrm{P}$ of the isolated-ion $^4F_{3/2}(1) \rightarrow {}^4I_{9/2}(1)$ CF transition and its satellites at 5 K. The splitting Δ_0 of the satellites with respect to the isolated-ion emission and the related pressure coefficients are also listed. Corresponding results for the isolated-ion $^4F_{3/2}(1) \rightarrow {}^4I_{11/2}(2)$ CF transition and its high energy (HE) and low energy (LE) satellites are also reported. All pressure coefficients result from linear regressions using data measured up to 5 GPa.

Final state	E_0^i cm^{-1}	$dE^i/d\mathrm{P}$ cm^{-1}/GPa	Δ_0 cm^{-1}	$d\Delta/d\mathrm{P}$ cm^{-1}/GPa
1/2 J_3	11 540.16(6)	−0.063(6)	+1.40(7)	+0.061(10)
1/2 J_2	11 539.61(3)	−0.096(7)	+0.85(4)	+0.028(11)
1/2 J_1	11 539.22(8)	−0.098(8)	+0.46(9)	+0.026(11)
$^4I_{9/2}(1)$	11 538.76(1)	−0.124(5)		
3/2 J_1	11 537.26(5)	[a]	−1.50(6)	[a]
3/2 J_2	11 536.46(2)	−0.270(4)	−2.30(3)	−0.132(8)
3/2 J_3	11 534.16(6)	−0.324(6)	−4.60(7)	−0.200(10)
HE	9497.68(5)	−2.66(5)	+1.63(9)	+0.07(1)
$^4I_{11/2}(2)$	9496.05(4)	−2.67(5)		
LE	9494.60(7)	−3.15(7)	−1.45(11)	−0.48(6)

[a]Uncertain because of energetic overlap with laser plasma line.

isolated ion emission consists of the same three components present in the low-pressure spectra. Of course, due to the broadening, the energies become less well defined compared to the situation at low pressures. The energy, width, and amplitude parameters, however, showed a regular behavior with pressure. The feature assigned as 3/2 J_1 in the ambient pressure spectrum in Fig. 2(b) becomes partly masked by the laser plasma line at higher pressures and therefore its energy shift with pressure cannot be determined with sufficient accuracy.

The change in pressure shift of the $^4F_{3/2}(1) \rightarrow {}^4I_{9/2}(1)$ transition near 5.5 GPa is clearly evident from Fig. 2(b). This also applies to the well resolved low-energy 3/2 J_2 and the weak 3/2 J_3 satellite. The overall pressure dependence of the $^4F_{3/2}(1) \rightarrow {}^4I_{9/2}(1)$ energy is very weak in the full pressure range up to 10 GPa, indicating a near cancellation of pressure effects on the Slater free-ion parameters, spin-orbit parameters, and crystal field strength.

An interpretation of the subtle change in pressure shift of the $^4F_{3/2}(1) \rightarrow {}^4I_{9/2}(1)$ emission near 5.5 GPa in terms of a structural phase transition, which involves some major volume or local coordination change, appears highly unlikely because of the continuous changes in energies and line widths of the luminescence bands. The change near 5.5 GPa from redshift to blueshift rather indicates a slight variation in

TABLE II. Ambient-pressure energies and energy pressure coefficients of the isolated-ion $^4F_{3/2}(1) \rightarrow {}^4I_{9/2}$ and $^4F_{3/2}(1) \rightarrow {}^4I_{11/2}$ CF transitions at 5 K. Energies of the $^4I_J(n)$ levels with respect to the ground state level $^4I_{9/2}(1)$ and corresponding pressure coefficients are also listed. Pressure coefficients correspond to the (initial) slopes of the solid lines in Figs. 4(a) and 4(b).

Final state	E_0^i cm^{-1}	dE^i/dP cm^{-1}/GPa	$E(^4I_J)$ cm^{-1}	$dE(^4I_J)/dP$ cm^{-1}/GPa
$^4I_{9/2}(1)$	11 538.76(1)	−0.124(2)	0	0
$^4I_{9/2}(2)$	11 406.80(5)	−2.00(8)	132.0(1)	1.88(10)
$^4I_{9/2}(3)$	11 355.70(4)	−3.53(6)	183.1(1)	3.41(8)
$^4I_{9/2}(4)$	11 291.08(6)	−4.60(4)	247.7(1)	4.48(6)
$^4I_{9/2}(5)$	11 010.93(8)	−10.54(2)	527.8(1)	10.42(4)
$^4I_{11/2}(1)$	9538.99(6)	−2.14(7)	1999.8(1)	2.02(9)
$^4I_{11/2}(2)$	9496.05(4)	−2.67(5)	2042.7(1)	2.55(7)
$^4I_{11/2}(3)$	9493.69(7)	−3.67(6)	2045.1(1)	3.55(8)
$^4I_{11/2}(4)$	9458.04(6)	−2.64(6)	2080.7(1)	2.52(8)
$^4I_{11/2}(5)$	9308.72(8)	−5.76(3)	2230.0(1)	5.64(5)
$^4I_{11/2}(6)$	9274.59(7)	−5.86(3)	2264.2(1)	5.74(5)

the local compressibility or coordination around the Nd^{3+} site and/or a change in the axial ratio. Differences in the local compressibilities around Y^{3+} and Li^+ may play a role.[26] Qualitatively similar explanations were offered for the decrease of the splitting of the two $^4F_{3/2}$ multiplets of Nd^{3+} in garnets[27] and for the change for some luminescence lines in chromium-doped Mg_2SiO_4 (forsterite) from blueshift to redshift with increasing pressure.[28] It was pointed out by Shen and Bray[28] that in forsterite the increase of the cubic field component in the C_s-site symmetry of the Cr^{4+} ion leads to an increase of the energy of some emission energies, whereas the increase of the noncubic CF component leads to a decrease of the energies. Therefore, depending on the relative influence of pressure in the cubic and noncubic field, one may observe either a redshift or a blueshift as a function of pressure.

The change in pressure shift of the $^4F_{3/2}(1) \rightarrow {}^4I_{9/2}(1)$ near 5.5 GPa ($T=5$ K) may be related to the changes in pressure coefficients reported for Raman mode frequencies at around 7 GPa ($T=300$ K).[22] There remains, however, some ambiguity about the interpretation of the Raman anomalies in relation to the present luminescence studies and those reported in Ref. 21.

The intensity of the $^4F_{3/2}(1) \rightarrow {}^4I_{9/2}(1)$ isolated-ion emission band was observed to vary linearly with the excitation density up to 100 kW/cm^2. Above this power density level saturation sets in. The intensity of the 3/2 J_2 satellite emission band also increases linearly with excitation density, at least up to 200 kW/cm^2. Higher power levels lead to an irreversible damage of the sample. The linear dependence of the luminescence intensity on excitation density, as observed in our 2% Nd-doped $YLiF_4$ sample, contrasts with the bistability effect associated with the Yb^{3+} pair satellite band in $CsCdBr_3:Yb$.[20]

Absence of intrinsic optical bistability associated with the 3/2 J_2 satellite confirms that short range interaction, of possible dipole-dipole character, is crucial for the bistability. This could be the reason why bistability is not observed with the 3/2 J_2 satellite which does not correspond to the closest pair as indicated by the stronger exchange interaction satellite 3/2 J_3 and the recently observed 3/2 J_4 satellite.[29]

B. Satellites of the $^4F_{3/2}(1) \rightarrow {}^4I_{9/2}(1)$ transition

We now consider the splittings Δ between the $^4F_{3/2}(1) \rightarrow {}^4I_{9/2}(1)$ central band and its satellites as a function of pressure. The predictions of the pair model, with its $E^i + J/2$ and $E^i - 3J/2$ doublet ground state splitting, remain valid when J increases under pressure. Values of the ambient-pressure splittings Δ_0 and pressure coefficients $d\Delta/dP$ are listed in Table I. For the satellites the absolute values of the splitting increases with pressure and the *relative* change is particularly large up to 5.5 GPa. This is very clearly seen for the 3/2 J_2 and 3/2 J_3 satellites. At ambient pressure, the coupling is ferromagnetic. Obviously, this coupling increases under pressure. A useful parameter in this context is the relative change of Δ with relative volume change

$$\gamma = -\frac{d\ln|\Delta|}{d\ln V} = \frac{B_0}{\Delta_0}\frac{d\Delta}{dP}.$$

For estimating γ we assume an ambient-pressure bulk modulus of $B_0 = 80$ GPa.[30] The pressure coefficients of the well-defined 3/2 J_2 and 3/2 J_3 sidebands give γ values of 5.1(4) and 3.5(4), respectively. These rather large values may indicate an unusually strong dependence of the magnetic interaction on the Nd^{3+}-Nd^{3+} pair distances. An additional or alternative possibility is that the ferromagnetic coupling between Nd ions is highly sensitive to small changes in Nd-F-Nd bond angles, which are about 110° at ambient conditions. Again, this would be related to different local compressibilities of NdF_8 and LiF_4 polyhedra.

The pressure coefficients dJ_i/dP are positive below 5.5 GPa. This indicates that the pair exchange interaction conserves, under pressure, its character with a spacing between the Nd^{3+}-Nd^{3+} ions kept above the minimum value required for ferromagnetic exchange integrals. The J_i become less sensitive to pressure above 5.5 GPa, possibly due to changes in the Nd^{3+} ion environment. A specific modeling of the pair exchange interaction, with a set of exchange-potential parameters (Ref. 31), should reflect the anisotropy that arises from the dependence on the orbital state of the Nd^{3+} ion and its evolution with pressure which is by far more complex than the phenomenological effective spin model adopted by Guillot-Noël *et al.* for the pair interactions.[17]

C. Other transitions originating from the $^4F_{3/2}(1)$ state

Luminescence spectra for some of the $^4F_{3/2}(1) \rightarrow {}^4I_{11/2}$ transitions at different pressures are shown in Fig. 3(a). The central band located at 9497 cm^{-1} at ambient pressure corresponds to the $^4F_{3/2}(1) \rightarrow {}^4I_{11/2}(2)$ CF transition, which is one of the laser emission lines of $YLiF_4:Nd$. Two additional bands near the laser emission line were observed at all pressures. These bands could reflect the Nd^{3+}-Nd^{3+} exchange

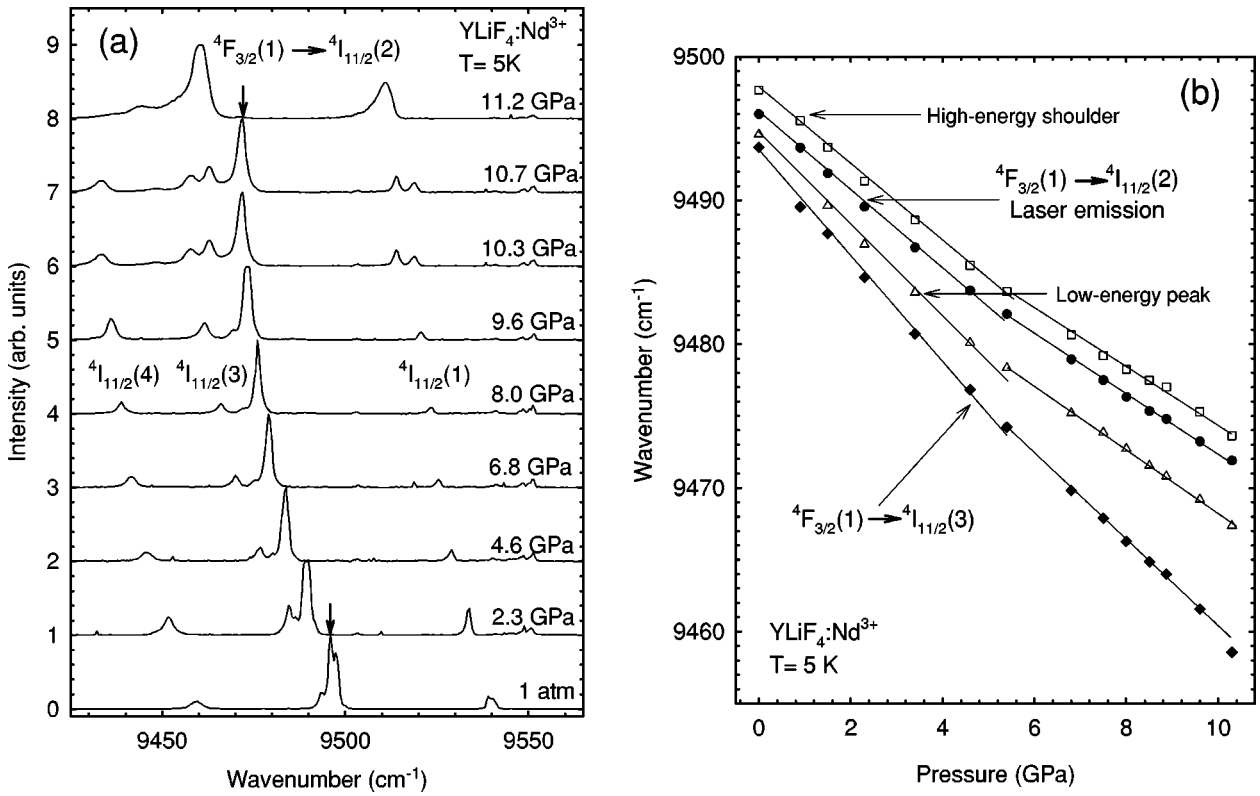

FIG. 3. (a) Luminescence spectra for $^4F_{3/2}(1) \rightarrow {}^4I_{11/2}$ transitions in $YLiF_4$:Nd at different pressures. Arrows mark the $^4F_{3/2}(1) \rightarrow {}^4I_{11/2}$ (2) laser emission line at 1 atm (9496 cm^{-1}) and 10.7 GPa (9472 cm^{-1}). The emission bands at 9539, 9493.7, and 9458 cm^{-1} at zero pressure correspond to the $^4F_{3/2}(1) \rightarrow {}^4I_{11/2}(n)$ transitions for $n=1$, $n=3$, and $n=4$, respectively. New peaks observed at pressures above 10 GPa are attributed to a structural phase transition. (b) Energies of the isolated-ion $^4F_{3/2}(1) \rightarrow {}^4I_{11/2}(2)$ (solid circles) and $^4F_{3/2}(1) \rightarrow {}^4I_{11/2}(3)$ transitions (solid diamonds) as a function of pressure. The $^4F_{3/2}(1) \rightarrow {}^4I_{11/2}(2)$ laser emission shows bands at its high- and low-energy side, marked by open squares and triangles, respectively.

interaction on the excited CF multiplet that was neglected in the ferromagnetic exchange interaction model of Guillot *et al.*[17,18] All luminescence lines seen in Fig. 3(a) show a pronounced red shift with increasing pressure. Note that the absolute shifts are much larger than those of the $^4F_{3/2}(1) \rightarrow {}^4I_{9/2}(1)$ related features (Fig. 2).

Figure 3(b) shows the energies of the $^4F_{3/2}(1) \rightarrow {}^4I_{11/2}(2)$ and $^4F_{3/2}(1) \rightarrow {}^4I_{11/2}(3)$ CF transitions as a function of pressure. As in Fig. 2(b), solid symbols refer to the energies of clearly resolved peaks, whereas the open symbols indicate the energies of additional Voigt lines used in fitting the side bands of the laser emission line. The pressure dependence of the energies in Fig. 3(b) can be described by a quadratic relation over the full range up to 10 GPa. However, the rather well defined point where the $^4F_{3/2}(1) \rightarrow {}^4I_{9/2}(1)$ changes slope [see Fig. 2(b)] suggests to also consider two separate pressure regimes for the other CF transitions. It is for this reason that we have indicated two different linear slopes in Fig. 3(b), corresponding to pressures below and above 5.5 GPa. Values of the ambient-pressure energies, linear pressure coefficients, and the relative change of the energy with volume for the $^4F_{3/2}(1) \rightarrow {}^4I_{11/2}(2)$ isolated-ion emission line and its satellites are included in Table I.

Figures 4(a) and 4(b) show the energies of all observed $^4F_{3/2}(1) \rightarrow {}^4I_{9/2}$ and $^4F_{3/2}(1) \rightarrow {}^4I_{11/2}$ isolated-ion emissions as a function of pressure. In the studied pressure range, all luminescence lines, except for the $^4F_{3/2}(1) \rightarrow {}^4I_{9/2}(1)$ emission, exhibit a pronounced shift to lower energies. The lower the $^4F_{3/2}(1) \rightarrow {}^4I_J(n)$ transition energy for a given J the larger is the red shift. This effect is mainly due to the increase in the CF splittings as pressure increases. A similar behavior has, for instance, been observed for Tm^{3+} and Cr^{3+} in YAG.[32,33] The ambient-pressure energies and the pressure coefficients of all observed transitions are summarized in Table II. Our ambient-pressure energy values compare well with the previously reported experimental and calculated values at 80 and 4.2 K.[10,34]

D. Pressure-induced phase transition

Above 10.3 GPa all luminescence lines were observed to undergo an abrupt change in energy and to broaden significantly [see, e.g., Fig. 3(a)]. Upon releasing pressure all the lines remained broadened and displaced in energy relative to the energies for the upstroke [see open symbols in Figs. 4(a) and 4(b)]. Upon fully releasing the pressure, however, the initial ambient-pressure energies were largely recovered. The abrupt change in the luminescence energies and the considerable hysteresis seen on decreasing pressure point to a structural phase transition occurring just above 10 GPa. The luminescence spectra indicate that the sample possibly reverts

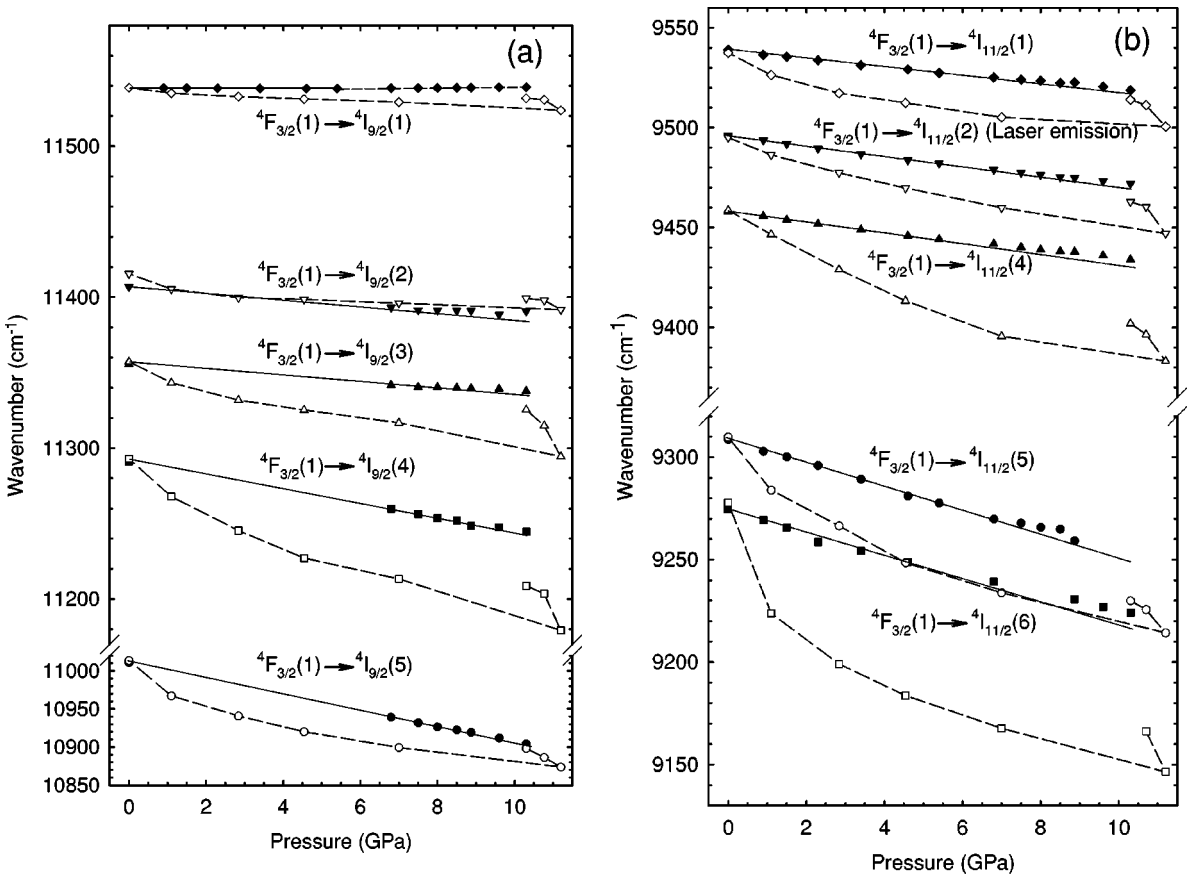

FIG. 4. Energies of luminescence peaks corresponding to transitions from the $^4F_{3/2}(1)$ excited state to the Stark levels of (a) $^4I_{9/2}$ and (b) $^4I_{11/2}$ states as a function of pressure. For the sake of clarity, the $^4F_{3/2}(1) \rightarrow {}^4I_{11/2}(3)$ transition, which is very close to the laser emission band ($\Delta E = 2.4$ cm^{-1}), is omitted in (b). The open symbols refer to data obtained after passing through the phase transition near 10 GPa and then releasing the pressure again.

to its original scheelite structure near ambient pressure with the persistence of defects as indicated by the lack of transparency in visual observation and the appearance of new broad luminescence bands below 1 GPa.

A variety of phase transition sequences is known or has been discussed for scheelite-type compounds under pressure.[36–41] At this point any suggestion for the structure of the high pressure phase of $YLiF_4$ is somewhat speculative. For scheelite ABO_4 compounds a pressure-induced transformation to the wolframite structure would be favored by packing-efficiency considerations.[36] However, as observed in Fig. 4 the energies of all the luminescence lines in the high-pressure phase of $YLiF_4$ show a shift on releasing pressure which is similar to the behavior in the scheelite structure for increasing pressure. These features indicate that the local environment of Nd in the high-pressure phase may not be very different from that of the scheelite phase. We believe this rules out a transition to the wolframite structure or distorted variants ($MnLiF_4$ or $HgMoO_4$ type) with an effective sixfold coordination of Y. On the other hand, based on ionic radius considerations and the Fukunaga-Yamaoka diagram,[38] a transformation of $YLiF_4$ to the monoclinic fergusonite structure or related low-symmetry structures could be expected. The transition between scheelite and *M*-fergusonite phases involves only small changes in the atomic coordinates.[42] The CF strength around the Nd^{3+} ions in the *M*-fergusonite and in the scheelite is expected to be similar because the coordination of Y^{3+} ions by F^- ions is not very different in both structures. This would explain the similar energy values for the high-pressure and scheelite phases. This argument, however, would also apply if the high-pressure phase would have a distorted scheelite structure of the $AgMnO_4$ variant or related to that of the high-pressure phase $BaWO_4$-II.[37]

IV. CONCLUSIONS

We have studied the pressure dependence of the $^4F_{3/2}(1) \rightarrow {}^4I_{9/2}$ and the $^4F_{3/2}(1) \rightarrow {}^4I_{11/2}Nd^{3+}$ CF transitions in $YLiF_4$, with emphasis on the $^4F_{3/2}(1) \rightarrow {}^4I_{11/2}(2)$ laser transition and on satellites of the $^4F_{3/2}(1) \rightarrow {}^4I_{9/2}(1)$ transition. The behavior of $^4F_{3/2}(1) \rightarrow {}^4I_{9/2}(1)$ satellites indicates a significant increase of the Nd^{3+}-Nd^{3+} ferromagnetic exchange interaction as the distance between pairs decreases. The observation of satellites of the $^4F_{3/2}(1) \rightarrow {}^4I_{11/2}(2)$ CF transition suggests that the splitting of the $^4F_{3/2}(1)$ multiplet as a consequence of the exchange interaction is not negligible as assumed before, but should be included in the exchange Hamiltonian of the coupled pairs. In addition to a possible use of the angular-overlap model to describe the isolated-ion CF transitions as proposed by Tro-

ester *et al.*,[35] the evolution of the satellite energies with pressure and the strong dependence of their magnetic interaction on the Nd^{3+}-Nd^{3+} intrapair distances constitute an experimental basis for the determination of the exchange-potential parameters and for *ab initio* calculations associated with anisotropic pair exchange interactions in solid state laser materials.

The luminescence spectra indicate that slight changes in the scheelite structure occur around 5.5 GPa. Discontinuous spectral changes near 10 GPa, also observed by Shenxin *et al.*[21] for $YLiF_4$:Eu, are attributed to a structural phase transition. A determination of lattice parameters and internal structural parameters of the scheelite phase as a function of pressure would be helpful for the theoretical modeling of the CF transitions and satellites under pressure. The structural character of the phase transition near 10 GPa is an interesting topic in itself which deserves being studied because of a possible relation to similar phase transitions in ABO_4 ternary oxides.

ACKNOWLEDGMENTS

F.J.M. acknowledges financial support from the European Union under Contract No. HPMF-CT-1999-00074. S.J. acknowledges support from the National Science and Engineering Research Council of Canada and le Fond de Formation de Chercheurs et l'aide a la recherche du gouvernement du Quebec. The authors thank U. Oelke for technical assistance.

*Present address: Applied Physics Department, Technical University of Valencia, E. P. S. A., Pl. Ferrándiz i Carbonell, 2 E-03801 Alcoy (SPAIN).

†Corresponding author; Email address k@syassen.de

[1] S. Preziosi, R.R. Soden, and L.G. Van Uitert, J. Appl. Phys. **33**, 1893 (1962).

[2] A.L. Harmer, A. Linz, and D.R. Gabbe, J. Phys. Chem. Solids **30**, 1483 (1969).

[3] S.J. Coe, P. Maine, and P. Bado, J. Opt. Soc. Am. B **5**, 2560 (1988).

[4] T. M. Baer, European Patent Application No. 87311280.9, 1988 (unpublished).

[5] T. Juhasz, S.T. Lai, and M.A. Pessot, Opt. Lett. **15**, 1458 (1990).

[6] A. A. Kaminskii, *Laser Crystals*, 2nd ed. (Springer, Berlin, 1990), and references therein.

[7] J.E. Murray, IEEE J. Quantum Electron. **QE-19**, 488 (1983).

[8] Z. Kollia, E. Sarantopoulou, A.C. Cefalas, M.A. Dubinskii, C.A. Nicolaides, R.Yu. Abdulsabirov, S.L. Korableva, A.K. Naumov, and V.V. Shemashko, J. Opt. Soc. Am. B **12**, 782 (1995).

[9] M. Malinowski, B. Jacquier, M. Bouazaoui, M.F. Joubert, and C. Linares, Phys. Rev. B **41**, 31 (1990).

[10] F.G. Anderson, H. Weidner, P.L. Summers, and R.E. Peale, J. Lumin. **62**, 77 (1994).

[11] L.C. Courrol, E.P. Maldonado, L. Gomes, N.D. Viera, I.M. Ranieri, and S.P. Morato, Opt. Mater. **14**, 81 (2000).

[12] S.P. Porto and J.F. Scott, Phys. Rev. **157**, 716 (1967).

[13] A.A.S. da Gama, G.F. de Sa, P. Porcher, and P. Caro, J. Chem. Phys. **75**, 2583 (1981).

[14] C.K. Jayasankar, F.S. Richardson, M.F. Reid, P. Porcher, and P. Caro, Inorg. Chim. Acta **287-290**, 139 (1987).

[15] R.B. Barthem, R. Buisson, J.C. Vial, and H. Harmand, J. Lumin. **34**, 295 (1986).

[16] O. Guillot-Noël, B. Viana, B. Bellamy, D. Gourier, G.B. Zogo-MBoulou, and S. Jandl, Opt. Mater. **13**, 427 (2000).

[17] O. Guillot-Noël, V. Mehta, B. Viana, D. Gourier, M. Boukhris, and S. Jandl, Phys. Rev. B **61**, 15338 (2000).

[18] V. Mehta, O. Guillot-Noël, D. Gourier, Z. Ichalalène, M. Castonguay, and S. Jandl, J. Phys.: Condens. Matter **12**, 7149 (2000).

[19] C.M. Bowden and C.C. Sung, Phys. Rev. A **19**, 2392 (1979).

[20] M.P. Hehlen, A. Kuditcher, S.C. Rand, and S.R. Lüthi, Phys. Rev. Lett. **82**, 3050 (1999).

[21] L. Shenxin, C. Yuanbin, Z. Xuyi, and W. Lizhong, J. Alloys Compd. **255**, 1 (1997).

[22] E. Sarantopoulou, Y.S. Raptis, E. Zouboulis, and C. Raptis, Phys. Rev. B **59**, 4154 (1999).

[23] G.J. Piermarini, S. Block, J.D. Barnett, and R.A. Forman, J. Appl. Phys. **46**, 2774 (1975).

[24] H.K. Mao, J. Xu, and P.M. Bell, J. Geophys. Res. **91**, 4673 (1986).

[25] S. Buchsbaum, R.L. Mills, and D. Schiferl, J. Phys. Chem. **88**, 2522 (1984).

[26] R.M. Hazen, L.W. Finger, and J.W.E. Mariathasan, J. Phys. Chem. Solids **46**, 253 (1985).

[27] H. Hua, S. Mirov, and Y.K. Vohra, Phys. Rev. B **54**, 6200 (1996).

[28] Y.R. Shen and K.L. Bray, Phys. Rev. Lett. **84**, 3990 (2000).

[29] M. Boukhris, S. Jandl, O. Guillot-Noël, and D. Gourier (unpublished).

[30] P. Blanchfield, G.A. Saunders, and Tu Hailing, J. Phys. C **15**, 2081 (1982).

[31] P.M. Levy, Phys. Rev. **135**, A155 (1964).

[32] P.R. Wamsley and K.L. Bray, J. Lumin. **60&61**, 188 (1994).

[33] Y.R. Shen and K.L. Bray, Phys. Rev. B **56**, 10882 (1997).

[34] H. De Leebeeck, K. Binnemans, and C. Gorller-Wallrand, J. Alloys Compd. **291**, 300 (1999).

[35] Th. Tröster, W.B. Holzapfel, and J. Goffart, Phys. Rev. B **51**, 14 892 (1995).

[36] A.W. Sleight, Acta Crystallogr., Sect. B: Struct. Crystallogr. Cryst. Chem. **28**, 2899 (1972).

[37] T. Fujita, S. Yamaoka, and O. Fukunaga, Mater. Res. Bull. **9**, 141 (1974); I. Kawada, K. Kato, and T. Fujita, Acta Crystallogr., Sect. B: Struct. Crystallogr. Cryst. Chem. **30**, 2069 (1974).

[38] O. Fukunaga and S. Yamaoka, Phys. Chem. Miner. **5**, 167 (1979).

[39] A. Jayaraman, S.Y. Wang, and S.K. Sharma, Phys. Rev. B **52**, 9886 (1995).

[40] D. Christofilos, G.A. Kourouklis, and S. Ves, J. Phys. Chem. Solids **56**, 1125 (1995).

[41] S.R. Shieh, L.C. Ming, and A. Jayaraman, J. Phys. Chem. Solids **57**, 205 (1996).

[42] O. Muller and R. Roy, *The Major Ternary Structural Families* (Springer-Verlag, Berlin, 1974), p. 83.